Available online at www.sciencedirect.com
ScienceDirect
International Journal of Heat and Mass Transfer 50 (2007) 2883–2894
International Journal of HEAT and MASS TRANSFER
www.elsevier.com/locate/ijhmt

# Temperature distribution in a thin composite plate exposed to a concentrated heat source

C. Corlay, S.G. Advani *

*Department of Mechanical Engineering and Center for Composite Materials, University of Delaware, Newark, DE 19716, USA*

Received 11 July 2006; received in revised form 6 January 2007
Available online 21 March 2007

**Abstract**

This study focuses on measuring and predicting the temperature distribution in a composite panel exposed to a concentrated heat source. The two heat sources studied in this work are a radiant heater and a gas burner flame. The parameters that are varied are the material properties and geometry, heat flux and distance. Finite element method based software Wintherm is used to predict the temperature distribution. The predictions are dependent on the choice of how one models the convective heat transfer coefficient along the surface of the plate exposed to the heat source. For the gas burner, the boundary condition will change dramatically from the centerline to the outward edges of the plate due to the plume effect. Empirical expressions are used and modified to determinate the air temperature in the region between the source and the plate. This information is implemented in the boundary condition along the plate surface to predict the thermal history of the plate. The predicted results are compared with the experimental temperature distribution which is measured with an infra-red camera. A parametric study is conducted to identify important dimensionless numbers and their impact on the temperature history.


## 1. Introduction

The percentage of polymeric materials used in civil construction, airplanes, automotive and marine industry continues to increase. Their properties and performances are well known at ambient temperature but need to be characterized when exposed to high temperatures for short duration. Fire and high heat exposure for long durations will visibly damage the composite structure and will have to be replaced. However, the structure can be exposed to high heat due to fire in the proximity in a plane garage, a heating blanket, a jet engine exhaust for a short duration. In such cases when the damage is not visible, the key questions that arise are: has the polymer degraded due to the short exposure to high temperatures? To what extent are its physical and mechanical properties compromised? Therefore, heat damage assessment becomes an important requirement for composites materials that undergo high heat exposure. Short time exposure to fire or other concentrated heat sources may degrade the resin at certain locations if the resulting temperature of the thermoset resin is in proximity of its glass transition temperature, $T_g$ for a sustained time frame. The first step therefore is to be able to predict time temperature history of a composite structure that is exposed to a heat source as a function of the type of heat source, the distance of the heat source from the composite structure and the magnitude of the heat flux. In this study, we experimentally measure the temperature history of thin composite plates exposed to a flame and a radiant heater at various distances from the composite plate and at different intensities. These results are compared with a numerical model. Non-dimensional parameters that influence the time temperature history are identified.

The heat damage determination has been of interest for many years. In 1979 Greer [1] determined the thermal aging in graphite/epoxy materials. Many research projects studied mechanical and physical effects of heat exposure of composites materials [2–4]. Non-visible damage has attracted researchers' attention as it became evident that even if the

* Corresponding author. Tel.: +1 302 8318975; fax: +1 302 8313619.
*E-mail address:* advani@udel.edu (S.G. Advani).

0017-9310/$ - see front matter © 2007 Elsevier Ltd. All rights reserved.
doi:10.1016/j.ijheatmasstransfer.2007.01.014

**Nomenclature**

| | |
|---|---|
| $r$ | outward distance from the centerline of the impingement (cm) |
| $H$ | height of the gas burner flame (mm) |
| $w$ | nozzle exit diameter of the gas burner (mm) |
| $Q_f$ | heat release rate of the flame (W) |
| $D$ | distance between the plate and the heat source (mm) |
| $D_0$ | reference for distance-non-dimension use (here 150 mm) |
| Alpert@$Q_f$ | Alpert solution for a heat release rate $Q_f$ |
| Yokoi@$Q_f$ | Yokoi solution for a heat release rate $Q_f$ |
| $a_0$ | constant = 0.5 |
| $b_0$ | constant = 1.81195 |
| $T$ | surface temperature of the plate exposed to a heat source |
| $T_\infty$ | ambient temperature (°C) |
| $T_{cm}$ | maximum temperature in the boundary layer below the horizontal plate exposed to a gas burner flame |
| $T_s$ | heat radiant surface temperature (°C) |
| $T_{inf}$ | minimum air temperature in between the radiant heater and the plate (°C) |
| $\zeta$ | $=r/(ZC^{2/3})$ |
| $C$ | constant representing a proportional constant, $L = CZ$ |
| $L$ | mixing length of turbulence, $L = CZ$ |
| $Z$ | coordinate (m) |
| $\Delta T$ | temperature rise (K) |
| $C_p$ | heat capacity at constant pressure (J/kg K) |
| $\rho$ | fluid density (kg/m$^3$) |
| $g$ | gravitational acceleration (m/s$^2$) |
| $h$ | convection heat transfer coefficient (W/m$^2$ K) |
| $k$ | thermal conductivity (W/m K) |
| $e$ | plate thickness (mm) |
| $\sigma$ | Stefan–Boltzmann constant |
| $\theta_{cm}$ | non-dimensional free stream temperature |
| $\theta$ | non-dimensional surface temperature of a plate exposed to a gas flame |
| $X_0$ | half the length of the plate |
| $T_{max}$ | maximal temperature of the plate exposed to the gas flame |
| $q_i$ | net heat rate at which radiation leaves surface $i$ |
| $F_{ij}$ | view factors in the radiative heat transfer. |
| $J_i$ | radiative coefficients |
| $\varepsilon_i$ | emissivity of surface $i$ |
| $A_i$ | surface area of surface $i$ |
| $T_i$ | uniform temperature of surface $i$ |
| $N$ | number of surfaces |

material is not visibly damaged, its use might be questionable because of material properties degradation. For example, short time exposures to high heat fluxes can cause spikes in the temperature field and alter material properties without visibly damaging the composite. Non-visible damages are hard to detect and to characterize; the tendency has been to use Non-Destructive Evaluation techniques, such as ultrasonics, hardness testing [5,6], acoustic emission [7] and thermography [8]. New techniques such as the Diffusion Reflectance Infrared Technique (DRIFT) spectroscopy analysis has been investigated by Mehrkam in 1993 to detect heat damage in epoxy composites [9], and later on used by Powell in 1997 to map the damage on graphite/epoxy composites [10]. To determine heat damage due to short time exposure, one needs to develop a relationship between the $T_g$ of the resin and regions of the material and the time scale for which they are exposed above $T_g$. Hence the importance of predicting the temperature field in a composite as a function of type and time of exposure to the heat source, and geometric parameters such as the distance separating the heat source and the material.

Flow field temperatures and species concentration above a free concentrated heat source have been studied [11–14]. When a plate is placed horizontally in a fire plume, it creates a ceiling-jet which is a boundary layer along the horizontal plate with specific gas temperature and velocity values differing from the plume itself. The flow is deflected and convected outward along the plate. Many studies report experimental results of flame impingement heat transfer analysis [15–27]. Most of the reported studies are focused on determining the boundary layers properties and not on predicting the temperature of the plate itself. You [28] investigated in details ceiling flows induced by impinging fires and weak plumes. He correlated theoretical and experimental values for ceiling-jet temperatures, velocities, convective and radiative ceiling-heat fluxes as a function of ceiling height and heat release rate of the flame. Alpert [29] found empirical expressions that predict unconfined maximum ceiling-jet temperatures and velocities as a function of the radial distance from the centerline. We will use these expressions to apply the boundary conditions to determine the transient temperature distribution in the composite plate that is exposed to a small gas burner flame. Williamson [30] investigated temperature, heat flux and ignition propensity of a lighter flame and plume. He found that these measurements follow the turbulent plume scaling laws and compare well with large-scale fire measurements.

This work focuses on determination of numerical and experimental temperature of a composite plate that is exposed to a concentrated heat source. Two different heat sources are studied in order to compare and contract the radiative dominant exposure to a convective heat transfer dominant situation. For the same heat release rate, depending on the mode of heat transfer, from a gas burner flame,

or a radiant heater, the heat effect on the sample exposed does differ. A non-dimensionalization study is also presented to identify important parameters that influence the temperature distribution.

## 2. Thermal plume models

When a horizontal plate is exposed to a heat source, the local air properties in between the heat source and the plate are distinctly different from the ambient temperature in the room (see Fig. 1). The temperature of the material will strongly depend on the convective boundary conditions that take into account the air temperature in the vicinity of the plate (within the boundary layer of the plate). The air temperature will vary as a function of $r$, radial distance from the centerline of impingement of the plume. The difficulty is then to characterize the air temperature in the plume produced by the flame as a function of the heat release rate of the heat source, the distance between the heat source and the plate and the time of exposure.

Several studies focused on the characterization of the plume above a flame ranging from a large-scale fire [12] to a small heat flux such as a lighter flame [30]. Yokoi [31] determined empirically the velocity and the temperature of the air in a free plume from a gas burner flame at any location in a rising current. The thermal plume in free space has also been modeled by Hara and Kato [11] using the standard $k$–$\varepsilon$ model in 2004.

When a plate is in the zone of a free plume, the gas properties change. The maximum air temperature in the boundary layer formed by the impinging plume on the plate will be much higher compared to a free plume for the same original heat flux. Hence for our situation, thermal plume models that consider the presence of a horizontal screen are pertinent. Alpert [29] has modeled the maximum air temperature underneath the exposed plate with empirical equations. Alpert developed expressions for unconfined ceiling in a room big enough so that the surrounding environment is at a constant ambient temperature. The equations predict the maximum air temperature of the ceiling jet at any distances from the centerline as a function of the heat flux rate:

$$\frac{T_{cm}-T_\infty}{T_\infty}=0.0577\frac{\dot{Q}_f^{2/3}}{D^{5/3}}\quad \text{for } (r/D)<0.18 \tag{1}$$

$$\frac{T_{cm}-T_\infty}{T_\infty}=0.0184\frac{(\dot{Q}_f/r)^{2/3}}{D}\quad \text{for } (r/D)>0.18 \tag{2}$$

where $T_\infty$ is the ambient temperature, $T_{cm}$ is the maximum temperature in the ceiling-jet, $\dot{Q}$ is the fire heat-release rate, $r$ is the radial distance of sprinkler from fire axis, and $D$ is the distance of the plate from the heat source base. This model provides an approximation that depends on radial distance if $r/D$ is greater than 0.18 (Eq. (2)). For lower values, there is no dependence on the radial position (Eq. (1)). This approximation is made for large-scale fires, and so does not apply entirely for our case of gas burner flame where we are interested in predicting the variation of air temperature accurately even in the centerline region. The central region, or impingement region, can be approximated using a free thermal plume model. Combining the expressions from Alpert and equations that predict the gas temperature in a free plume, we can predict air temperatures underneath a plate exposed to a concentrated heat source such as the gas flame. We will use Yokoi [31] prediction for the impingement region as follows:

$$\Delta T=0.423\left[\frac{T_\infty Q^2}{C_p^2\rho^2 g}\right]^{1/3}C^{-8/9}Z^{-5/3}\times(1+0.9383\zeta^{3/2}+0.4002\zeta^3+0.0939\zeta^{9/2})\times\exp(-1.4617\zeta^{3/2}) \tag{3}$$

with $\zeta=r/(ZC^{2/3})$, $r$ represents the horizontal distance from the centerline of the heat source, $C$ is a constant representing a proportional constant under the assumption that the mixing length of turbulence $L$ is proportional to height $Z$, i.e., $L=CZ$. $\Delta T$ is the temperature rise (K), $C_p$ is the heat capacity at constant pressure (J/kg K), $\rho$ is the fluid density (kg/m$^3$), $T_\infty$ is the ambient temperature (K), $g$ is the gravitational acceleration (m/s$^2$) and $Z$ is the $z$ coordinate (m). The constant $C$ assumes different values depending upon the geometry of the heat source: $C^{2/3}=0.062$ for a point heat source and $C^{2/3}=0.1$ for a circular heat source with a finite radius. Several thermal plume models have been developed over the years. All of them focus on featuring different fire sizes and intensities, and

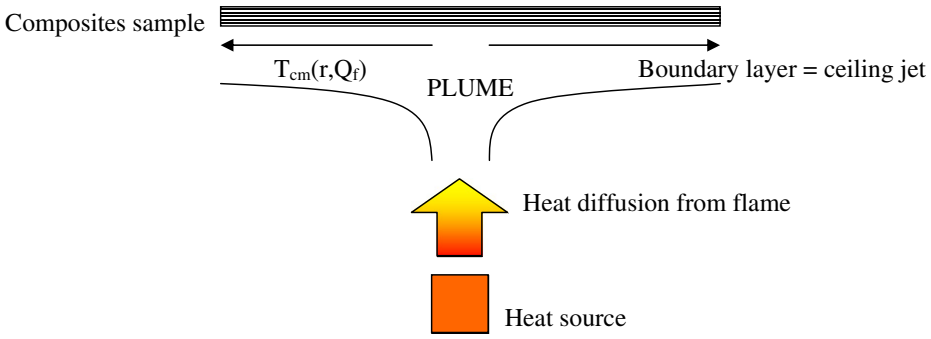


Fig. 1. Schematic depicting the change in air temperature due to a plume created by a gas source along a horizontal plate.

confinement conditions. To apply a thermal plume model to our experimental conditions, which is an exposure of unconfined composite plate to a concentrated heat source, we would have to carefully select the equation that closely represents our situation.

## 3. Experiments

A composite plate is exposed to a concentrated heat source. The goal is to measure experimentally the thermal history of the plate that is experiencing the heat. The range of time exposure is from 8 to 20 min (steady state is reached after 5 min). In order to compare the influence of different high heat sources on the plate, we used two different concentrated heat sources; a gas burner flame and a radiant heater electrical surface. For both cases we used an infra-red camera to record the thermal history of the exposed surface of the plate.

The plates were made from three different composite materials: (i) prepregs of carbon fibers and vinylester resin, (ii) carbon fibers and BMI resin, and (iii) fiberglass mats and epoxy resin. The intent was to also explore the role of the plate material on the temperature distribution. The average thickness of the plates was 3 mm. The plate was exposed to two types of concentrated heat sources: (i) gas burner and (ii) radiant heater.

## 4. Gas burner

The composite plate (270 by 270 mm) was exposed to a gas burner flame. The experimental parameters that were varied were (i) the horizontal distance, $D$ separating the gas burner from the plate, (ii) the dimensions of the flame (height $H$ and diameter of the base of the flame $w$) and (iii) the exposure time. Temperature distribution on the exposed surface was recorded with an infra-red camera placed on the floor facing the surface that is exposed to the heat source. The camera software [32] was adapted to record accurate temperature distribution which was validated with thermocouples placed at reference locations. The experimental set-up is shown in Fig. 2a.

The gas burner nozzle exit is 10 or 16 mm wide. The flame is characterized in a way that is easily reproducible. To characterize the flame, we use its height $H$ and the nozzle exit diameter $w$, characterizing the base of the flame dimension. The flame height is carefully measured in similar light environment using a scale. The heat release rate of each characteristic flame is determined from Alpert's equation (2) and summarized in Table 3. To make sure that the measurements are comparable, we always strain to retain same room conditions. The distance, $D$ was varied between 125 and 320 mm. The flame height was varied from 20 to 90 mm. The samples were exposed between 15 and 20 min. The steady state temperature is reached after

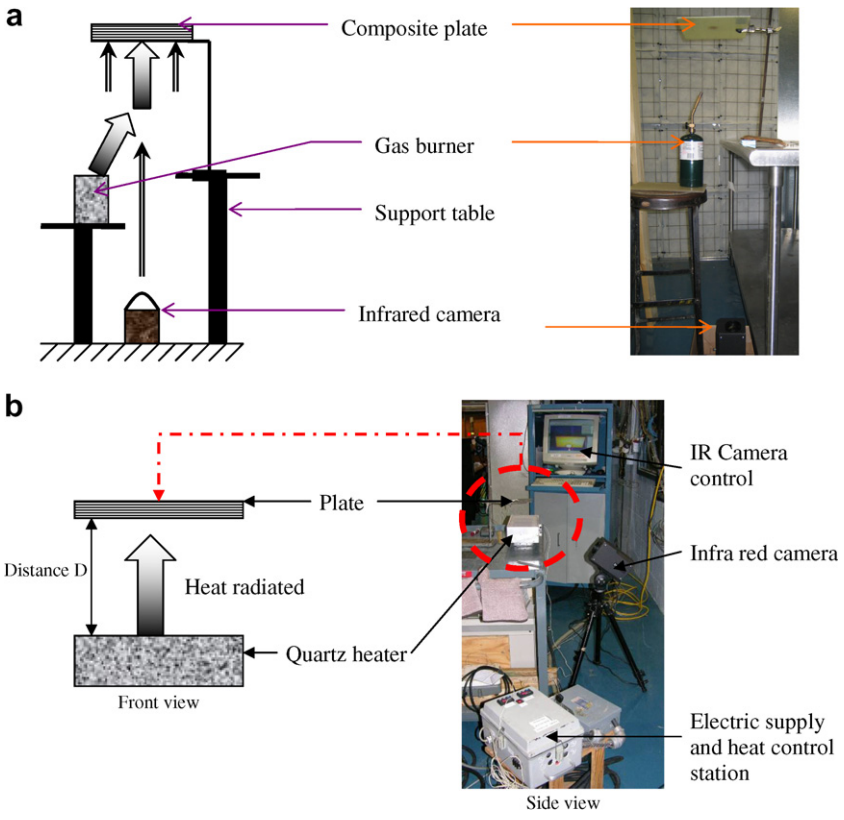


Fig. 2. Schematic and a snapshot of the experimental set-ups showing the flame (a) and radiant heater (b) exposures of the composite plate along with IR camera to record the two dimensional temperature distribution on the exposed surface of the plate.

Table 1
Gas burner experimental settings

| | Distance gas burner-plate, $D$ (mm) | Flame height, $H$ (mm) | Nozzle exit diameter $w$ (mm) | Material |
|---|---|---|---|---|
| GB 1 | 160 | 20 | 10 | Carbon fiber and vinylester |
| GB 2 | 320 | 20 | 10 | Carbon fiber and vinylester |
| GB 3 | 320 | 40 | 10 | Carbon fiber and vinylester |
| GB 4 | 150 | 80 | 10 | Carbon fiber and BMI |
| GB 5 | 125 | 80 | 10 | Carbon fiber and BMI |
| GB 6 | 200 | 90 | 16 | Carbon fiber and BMI |
| GB 7 | 215 | 90 | 16 | Glass fibers and epoxy |

5 min. The experimental conditions are summarized in Table 1.

## 5. Results

The temperature distribution collected by the infra-red camera as expected showed that the temperature was radially symmetric about the source which is the central impingement of the gas burner flame on the plate (Fig. 3). The results of the seven experiments are presented in Fig. 4a.

One can note that the temperature is inversely proportional to the distance from the flame tip and directly proportional to the flame height. The relationship is non-linear and weakly dependent on the material properties as well.

## 6. IR heater

Unlike the gas burner, the radiant heater provides the heat by radiative heat transfer. Hence it is interesting to compare two different sources of high heat flux and their influence on the temperature distribution of the plate. An electric quartz surface radiates heat uniformly on a 150 by 350 mm$^2$ surface area for the experiments. The experimental set up is similar to the gas burner experiments. The composite plate is exposed horizontally above the heat source at a distance $D$ (see Fig. 2b). We use also an infra-red camera facing the front side of the sample to record the temperature as a function of time in the plane of the composite. The plate size is identical to the heater size and hence one can expect the heating surface to have uniform temperature. The parameters that we vary from one experiment to the next are the distance from the heater D and the heat source temperature.

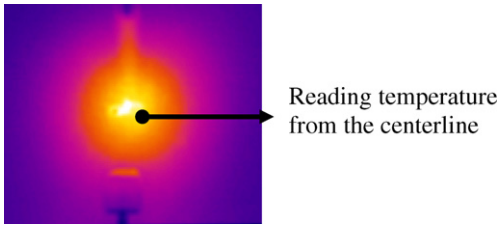


Fig. 3. Infra red camera picture of a flame exposed plate. From experiment GB5 after 20 min.

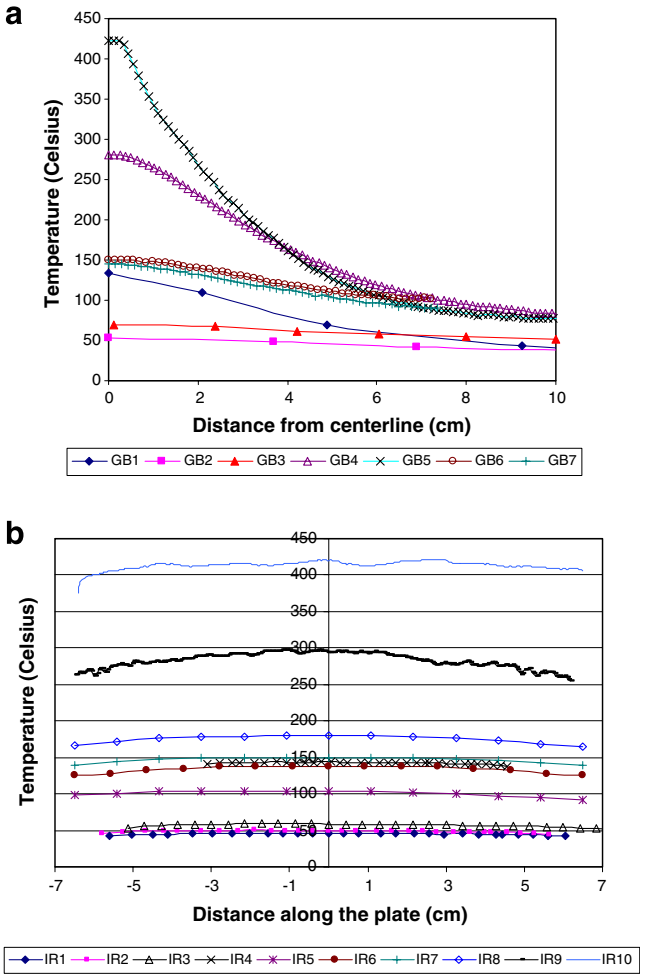


Fig. 4. Experimental temperature field on the exposed plate surface as measured by infra red camera: (a) flame exposure—the different experimental settings are listed in Table 1, the distance is measured from the point of impingement on the plate; (b) radiant heater exposure—the different experimental settings are listed in Table 2.

We are not interested in visibly damaging the sample, but in understanding the relation between the distance $D$, the temperature of the heat source and the temperature of the exposed plate surface. The temperature of the heat source varied between 280 °C and 700 °C. The range of distances separating the heater from the plate varied between 62 and 440 mm. The parameters for the experiments are summarized in Table 2.

The experimental results are presented in Fig. 4b. As expected the temperature increases when the distance separating the plate and the heat source decreases. Rate of increase in temperature is higher when the sample is closer than 200 mm from the heat source.

Table 2
Parameters for the IR heating experiments

| | Distance plate, $D$ (mm) | Heat source temperature, $T_s$ (°C) | Time of exposure (min) | Material |
|---|---|---|---|---|
| IR1 | 340 | 280 | 20 | Carbon vinylester |
| IR2 | 300 | 280 | 20 | Carbon vinylester |
| IR3 | 260 | 280 | 20 | Carbon vinylester |
| IR4 | 62 | 280 | 20 | Carbon vinylester |
| IR5 | 440 | 550 | 20 | Carbon vinylester |
| IR6 | 340 | 550 | 20 | Carbon vinylester |
| IR7 | 300 | 550 | 20 | Carbon vinylester |
| IR8 | 160 | 550 | 20 | Carbon vinylester |
| IR9 | 150 | 590 | 20 | Carbon BMI |
| IR10 | 75 | 700 | 1 | Carbon BMI |

## 7. Prediction of temperature distribution for a gas flame as concentrated source

When a plate is exposed to a gas flame, the sample temperatures vary along the plate from the impingement point as a function of the air properties located underneath the plate in the boundary layer formed by the plume impingement. To model this change in temperature on the plate, we simulate the heat transfer problem using a finite element method, as packaged in the software, WINTHERM [33]. The software WINTHERM uses the transient heat diffusion equation to describe the heat transfer within any material which interacts with its boundaries by radiation, convection and conduction. The temperature distribution for a simple geometrical was analytically calculated and compared with the WINTHERM results in order to validate the software. In the next section we also consider the case of a composite plate exposed to a radiant heat source at constant temperature. An analytical solution is presented that will also validate the numerical code used.

The plume effect is modeled as a change in air temperature in the boundary layer below the plate as a function of radial distance from the centerline of the impingement. This maximum air temperature which can be considered as the free stream temperature of air at the end of the boundary layer, $T_{cm}$ decreases as one moves outward from the impingement point. This temperature is used to supply the temperature for the convective boundary condition below the plate in the software. To estimate $T_{cm}$, one needs the following parameters: (i) heat release rate of the flame $Q_f$, (ii) the distance $D$ of the plate from the base of the flame, and (iii) the ambient temperature $T_\infty$.

In order to improve the model's applicability to any small-scale fire case, we provide a way to determine the heat release rate as a function of the geometry of the gas flame. For each gas flame height and width, a characteristic heat release rate is calculated. Using the presented model, we can determine the sample temperature while using Alpert result (Eq. (2)). Alpert equation asks for the heat release rate of the flame as an input. While varying the heat release rate input, one can match numerical and experimental results. When both match, we can assign the calculated heat release rate value for one flame geometry. Table 3 presents the heat release rate values that match for one physical geometry of the flame. For one flame geometry, we can therefore input a heat release rate value.

Table 3
Heat release rate values as a function of gas burner geometry flame

| Exit nozzle of 10 mm width | | Exit nozzle of 16 mm width | |
|---|---|---|---|
| Flame height, $h$ (mm) | $Q_f$ (W) | Flame height, $h$ (mm) | $Q_f$ (W) |
| 20 | 30 | 90 | 100 |
| 40 | 80 | | |
| 80 | 200 | | |

Wider base of the flame does not imply high heat release rate as evident from Table 3. Indeed, the geometry of the flame for an exit nozzle of 16 mm width provides a wider base but the width of the flame rapidly narrows down along the height of the flame. For the same flame height the heat release rate of the flame is therefore less for a wider nozzle exit diameter than for a narrower one. As explained in the thermal plume model paragraph, Alpert equation (2) approximates the maximum air temperature underneath a horizontal plate located in fire plume as a function of the outward distance from the centerline. Alpert approximation is originally made for large-scale flame. The application of this approximation to our small-scale gas burner flame will not give accurate temperature values in the centerline region. Therefore, we combined his expression with the approximation of Yokoi [31] for the thermal plume properties of a free flame. This is for our case of narrow flame, a good approximation applied in the centerline area. The presence of the plate in the plume increases the temperature of the air. Combining the two expressions (Alpert's and Yokoi) in a way that Alpert models the outward region, and Yokoi the central region we can write the following expression:

$$\frac{T_{cm}}{T_\infty} = \left( a_0 \left( \frac{\text{Alpert@}Q_f}{T_\infty} \right) + b_0 \left( \frac{\text{Yokoi@}Q_f}{T_\infty} \right)^{1.4} \right) \tag{4}$$

where $a_0$ and $b_0$ are found by correlation with previous experimental results ($a_0 = 0.5$ and $b_0 = 1.81195$). The needed inputs are the heat release rate of the flame $Q_f$, the plate distance $D$ from the heat source and the ambient temperature. A non-dimensional free stream temperature was defined as follows:

$$\theta_{cm} = \left( \frac{T_{cm} - T_{min}}{T_{max} - T_{min}} \right)^{\frac{D}{D_0}} \tag{5}$$

in which $T_{min}$ is the minimum temperature value, from Eq. (4), of the boundary layer created by a horizontal plate of 20 mm long. This minimum value is located under the edge of the exposed plate. $T_{max}$ is the maximum value found from Eq. (4) of the boundary layer and is located at the centerline of the ceiling jet impingement. $D$ is the distance separating the heat source and the sample and $D_0$ is a reference value equal to 200 mm. The non-dimensional free

stream temperature allows us to collapse all the results on one graph as shown in Fig. 5 for all the different parameter variations listed in Table 4.

Once the air temperature is determined for each exposure, it is used as a boundary condition in the finite element program to find the surface temperature distribution of the exposed surface of the plate. The program takes into account for the radiation, convection and conduction heat transfer modes. In the case of a gas flame exposure, the radiation of the concentrated flame can be neglected. Only convection and conduction are taken into account. Conductivity, emissivity, density and thermal conductivity value of the material are input in the software, those parameters are summarized in Table 5. We assign different free stream convective air temperatures to different parts of the plate. We divided the region from the center to the edge into five parts and assigned average value of free stream temperature as calculated from Eq. (4). An example of a typical numerical result for radial change in plate temperature from the point of impingement to the edge is shown in Fig. 6.

The continuity of the temperature values can be improved using more sections between the center and the edge to represent the convective free stream temperature of the air. The simulation provides temperature distribution for both the exposed and unexposed surface temperatures. The experimental and numerical comparison is in Fig. 7.

Numerical and experimental results correlate to various degree of accuracy depending on the intensity of the flame and the distance of the flame from the plate. The best results are obtained for small flame which is far away from the plate. Better approximations can be obtained by improving the simulation by providing more accurate description of air temperature below the plate by subdividing the plate into more regions. The emissivity approximations in the experimental part may also influence the final results. Eq. (4) is therefore a useful approximation of the maximum air temperature underneath an exposed plate that is input in the final simulation. For a given flame geometry, ambient temperature, distance and material properties one is able to predict the sample surface temperature.

An important non-dimensional parameter for the surface temperature is identified in Eq. (6):

$$\theta = \left(\frac{T - T_\infty}{T_{\max} - T_\infty}\right)^{\frac{D}{D_0}} \tag{6}$$

$T_\infty$ represents the ambient temperature in the room, $D$ is the distance between the plate and the heat source, $D_0$ is a reference distance equal to 155 mm. The resulting non-dimensional temperatures are presented in Fig. 8 as a function of non-dimensional distance from the center. $X_o$ is half the length of the plate.

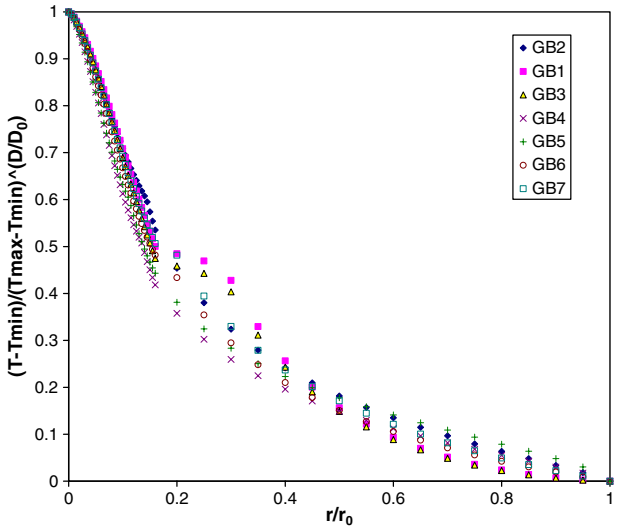


Fig. 5. Non-dimensional maximum air temperature in the ceiling jet of a small heat source exposure of a composite plate to a gas flame.

Table 4
Distance and heat release parameters for the seven experiments conducted

| | Distance, $D$ (mm) | Heat release, $Q$ (W) |
|---|---|---|
| GB1 | 160 | 30 |
| GB 2 | 320 | 30 |
| GB 3 | 320 | 80 |
| GB 4 | 150 | 200 |
| GB 5 | 125 | 200 |
| GB 6 | 200 | 100 |
| GB 7 | 215 | 100 |

Table 5
Input parameters for simulation Wintherm

| | |
|---|---|
| Emissivity | 0.9 |
| Thickness | 3 mm |
| Thermal conductivity | $k = 0.23$ W/m K |
| Convection coefficient | $h = 8$ W/m$^2$ K |
| Convective temperature | $T_{cm}$ |

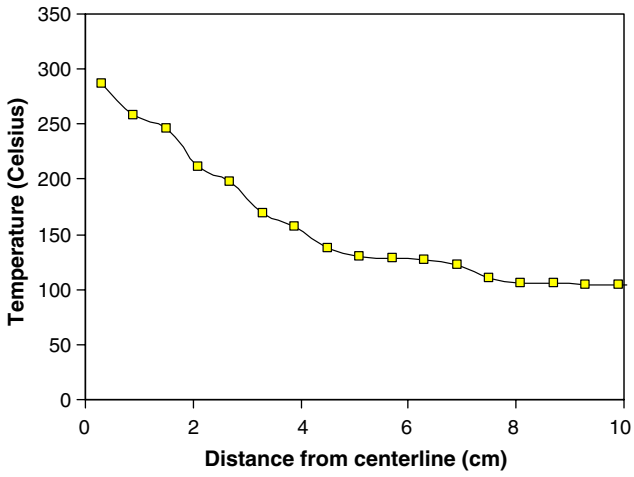


Fig. 6. Numerical surface temperature distribution of a plate exposed to a gas flame result from Wintherm software.

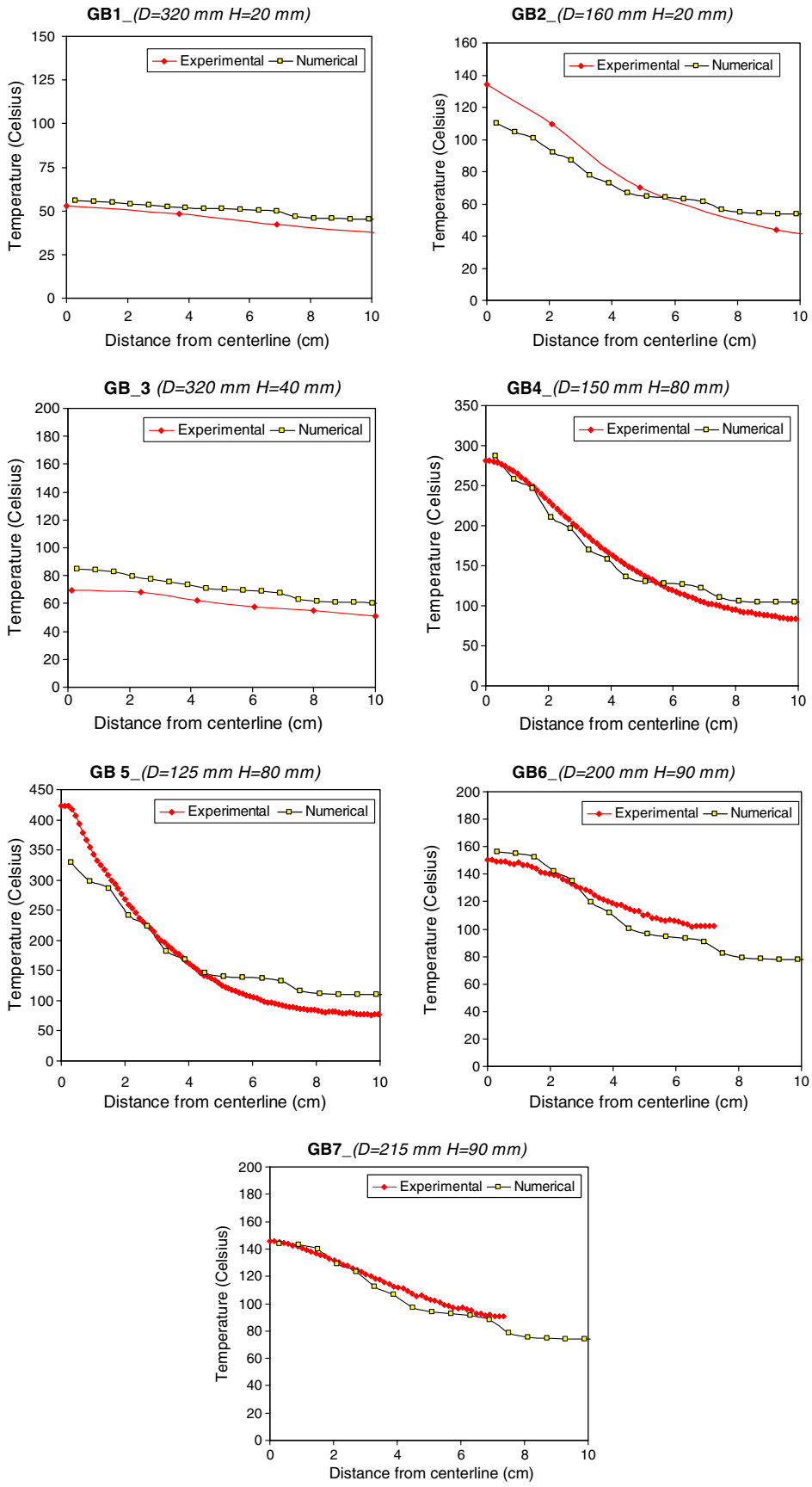


Fig. 7. Comparison of experimental and numerical results of radial temperatures of a composite plate exposed to a flame. The exposure conditions for the seven results GB1–GB7 presented above are listed in Table 1.

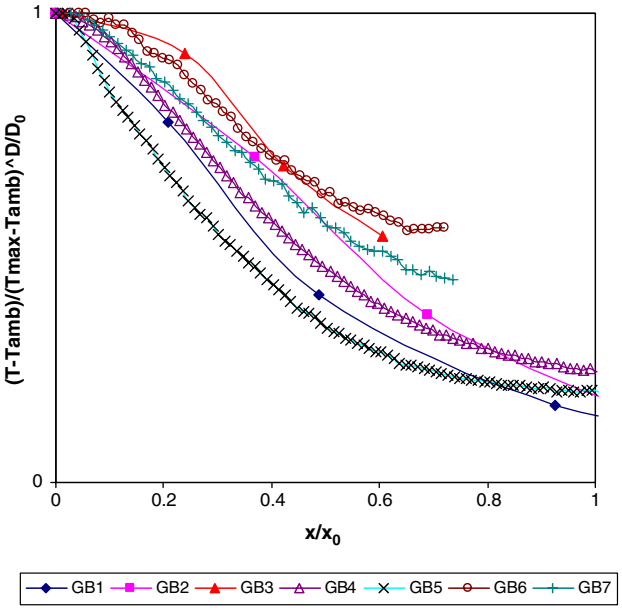


Fig. 8. Experimental temperature distributions for the gas burner experiments expressed in a non-dimensional way (Eq. (6)).

The non-dimensionalization shows how quickly the temperature of the plate changes as we move away from the center for small flames.

## 8. Prediction of temperature distribution for infra-red heater as concentrated heat source

The radiant heater dominant mode of heat transfer is radiation. Therefore, the approach to model the resulting thermal history will be different as compared to the gas burner.

We consider a simple case of a composite plate exposed to a radiant heat source at constant temperature. An analytical solution is presented that will validate the numerical code used. The plate temperature is assumed to be uniform, therefore the analytical solution is not an exact solution but an approximation. A three surfaces enclosure can be used to model the radiative heat transfer between the heater and the plate. For $N$ surfaces, the net heat rate $q_i$ at which radiation leaves surface $I$, including radiosity and irradiation is expressed as

$$q_i = \frac{Eb_i - J_i}{(1-\varepsilon_i)/\varepsilon_i A_i} \tag{7}$$

$$q_i = \sum_{j=1}^{N} A_i F_{ij}(J_i - J_j) = \sum_{j=1}^{N} q_{ij} \tag{8}$$

The view factors $F_{ij}$ depend on geometric factors such as the area of the plates and the distance from each other and can be found from any heat transfer text book [34]. For each of the surfaces in the enclosure, either $T_i$, the steady state temperature or $q_i$ the net heat rate of the surface $i$ are known. Based on electric analogy one can write and solve a set of linear equations to find $J$'s the radiosity of each surface. If $T_i$ is known, the following equation is used to find the unknown $J_j$:

$$\frac{Eb_i - J_i}{(1-\varepsilon_i)/\varepsilon_i A_i} = \sum_{j=1}^{N} \frac{J_i - J_j}{(A_i F_{ij})^{-1}} \tag{9}$$

If $q_i$ are known for the surface, the following equation is used to find the $J_s$:

$$q_i = \sum_{j=1}^{N} \frac{J_i - J_j}{(A_i F_{ij})^{-1}} = \sum_{j=1}^{N} q_{ij} \tag{10}$$

$q_{ij} = \frac{J_i - J_j}{(A_i F_{ij})^{-1}}$ is the net heat rate leaving from surface $i$ and arriving to surface $j$. Once $J_i$ are known, one can use Eq. (6) to find the temperature $T_i$ if $q_i$ is known.

This standard approach was applied to the radiant heater and the plate problem in which a few assumptions were made to obtain a closed form solution. We assumed that the composite plate and the heater have the same dimensions. The heat source temperature was assumed to be constant and known and does not change over time. The surfaces to be considered in the analysis are: the heater surface (1), both sides of the composite plate {the bottom (2) facing the heat source and the top(3)}, and the surroundings (4) considered as a blackbody. As radiative mode is at the speed of light, a steady state solution was sought.

The parameters to be considered: the distance $D$ separating the plate and the heater, the heat source temperature $T_s$, the ambient room temperature $T_\infty$, and the free stream temperature of the air $T_{\text{inf}}$ between the two plates. Input parameters for this case are summarized in Table 6. Two different regions are studied, one at a time. The back surface of the exposed face that is not facing the heater and the surrounding constitute the first region. In this case, we consider only two surfaces, the top surface, indexed as 3, and the surroundings, indexed as 4, which is considered as a blackbody. Using the energy balance at the surface 3 between the various modes of heat transfer as follows,

$$q_{\text{cond}} = q_{\text{rad}} + q_{\text{conv}} \tag{11}$$

We can express Eq. (11) in terms of temperature using the Fourier law of heat conduction, Newton law of cooling and Stefan's Boltzman law of radiation:

$$\frac{k(T_2 - T_3)}{e} = \varepsilon_3 \sigma (T_3^4 - T_4^4) + h(T_3 - T_4) \tag{12}$$

The two unknowns are the temperatures of the two surfaces of the plate ($T_2$ and $T_3$). $T_4$ is the ambient room temperature known as $T_\infty$. An additional equation is

Table 6
Boundary conditions—analytical study

| | |
|---|---|
| Stefan–Boltzmann constant | $\sigma = 5.67 \times 10^{-8}$ W/m$^2$ K$^4$ |
| Thickness | $e = 5$ mm |
| Thermal conductivity | $k = 0.4$ W/m K |
| Convection coefficient | $h = 5$ W/m$^2$ K |
| Emissivity | $\varepsilon = 0.9$ |
| Source temperature | $T_s = 280$ °C |

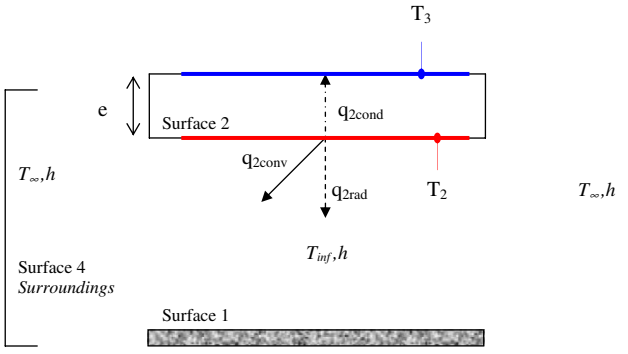


Fig. 9. Schematic of the three surfaces enclosure of the heat transfer calculations of a horizontal plate at a certain distance of a heating surface.

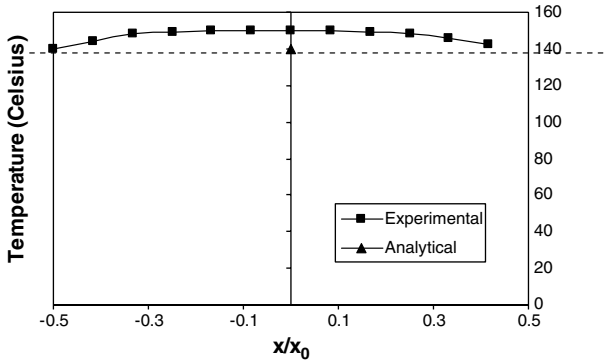


Fig. 10. Comparison between analytic and experimental temperature values on the composite plate surface exposed to an IR heater.

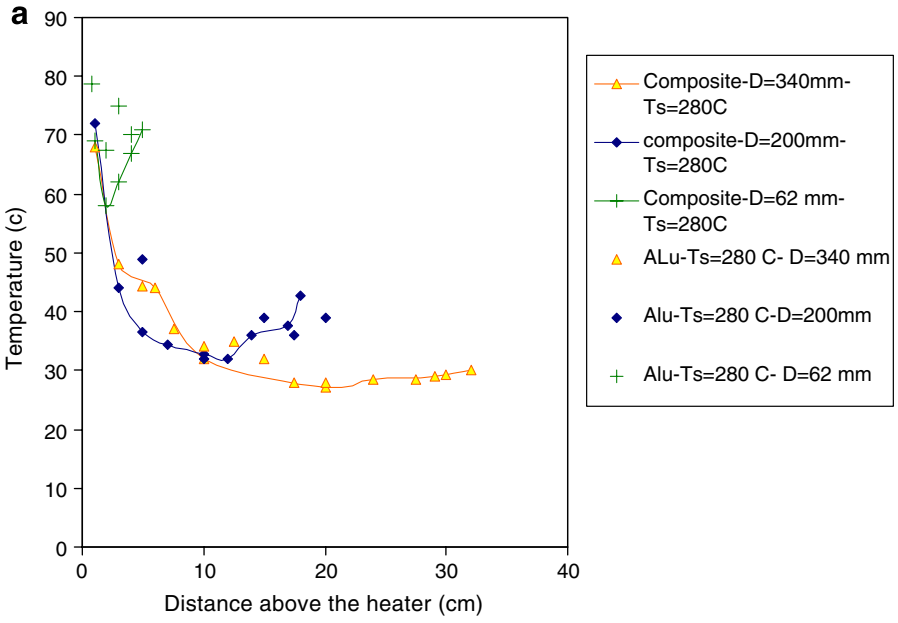


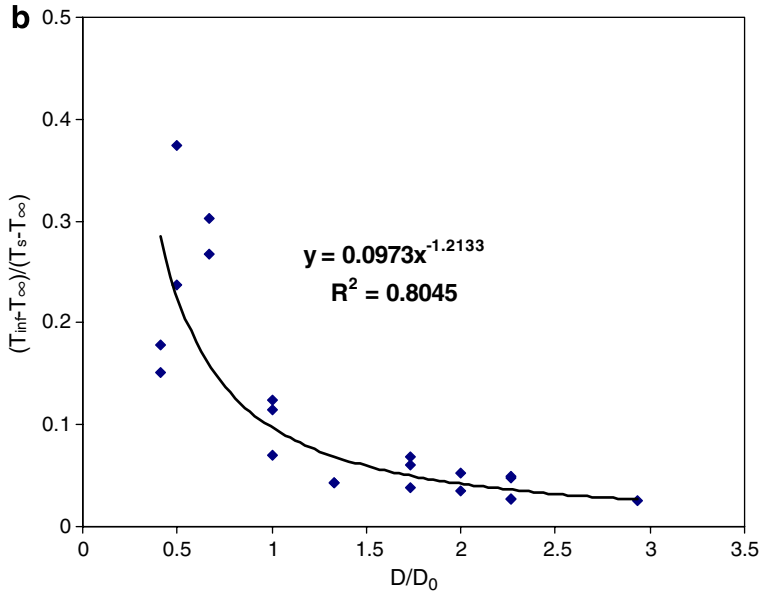


Fig. 11. (a) Air temperature data between the heater and the plate for different distance/heat source temperature conditions and different materials (composite and aluminum). (b) Non-dimensionalization and empirical correlation of the free stream temperature $T_{inf}$ between a radiant heater and a horizontal plate.

formulated by considering a three body enclosure consisting of: the heat source (surface 1), the exposed side of the plate (surface 2) and the surroundings (surface 4).

$$q_{2\text{conv}} + q_{2\text{rad}} + q_{2\text{cond}} = 0 \tag{13}$$

$$h(T_2 - T_{\text{inf}}) + \frac{Eb_2 - J_2}{(1-\varepsilon_2)/\varepsilon_2} = -k(T_2 - T_3)/e \tag{14}$$

The energy balance (13) is used at the exposed side of the plate as shown in Fig. 9 and expressed in terms of temperature and heat transfer parameters in Eq. (14). $T_{\text{inf}}$ is the free stream temperature between the two plates and is determined experimentally. The view factors are known from the geometric parameter (surface area of the plate, and distance between them), and are equal to $F_{21} = F_{12} = 0.14$; $F_{24} = 0.86$. Applying Eq. (9) to surfaces 1 and 2 we can find $J_1$ and $J_2$. Using $J_1$ and $J_2$ values, we can now solve for $T_2$ and $T_3$ from Eqs. (12) and (14). Fig. 10 presents a comparison between the analytical and the experimental result for the experiment IR7. The error between the analytical solution and the experimental one is within 5%. The experimental solution is not completely uniform along the plate length due to the edge effects which were not modeled in the analytic solution.

The free stream temperature in between the heat source and the plate, $T_{\text{inf}}$ is defined as the minimum air temperature along the imaginary line linking the middle of the heater and the middle of the exposed plate. To assess a free stream temperature as a function of plate distance and the heat source temperature, we experimentally measured the air temperature between the radiant heater and the plate with a thermocouple at different locations. For different materials, distances, and heat source temperature, the set of air temperatures were recorded (Fig. 11a).

It was found that the type of material exposed did not influence the air temperature for a plate thickness equal to 3 mm. For each set up the minimum temperature was noted as $T_{\text{inf}}$, the free stream temperature between the two plates. The set of $T_{\text{inf}}$ values obtained for the different heat sources temperature, different materials, and varying distances can be plotted as a function of distance of the plate from the heat source. A non-dimensional expression for the free stream temperature was formulated in Eq. (15) and the results are plotted in Fig. 11b.

$$\frac{T_{\text{inf}} - T_\infty}{T_s - T_\infty} = 0.0973\left(\frac{D}{D_0}\right)^{-1.2133} \tag{15}$$

The empirical non-dimensional equation (15) determines the minimum air temperature $T_{\text{inf}}$, between the heater and the sample as a function of the distance between the plate and the source temperature.

Once the free stream temperature is determined, we use the value in the finite element software Wintherm [33] to compute a temperature map of the sample exposed. The numerical results for the surface temperature are presented in Fig. 12a along with the experimental results. For the IR9 experiment, the back surface temperature is also presented

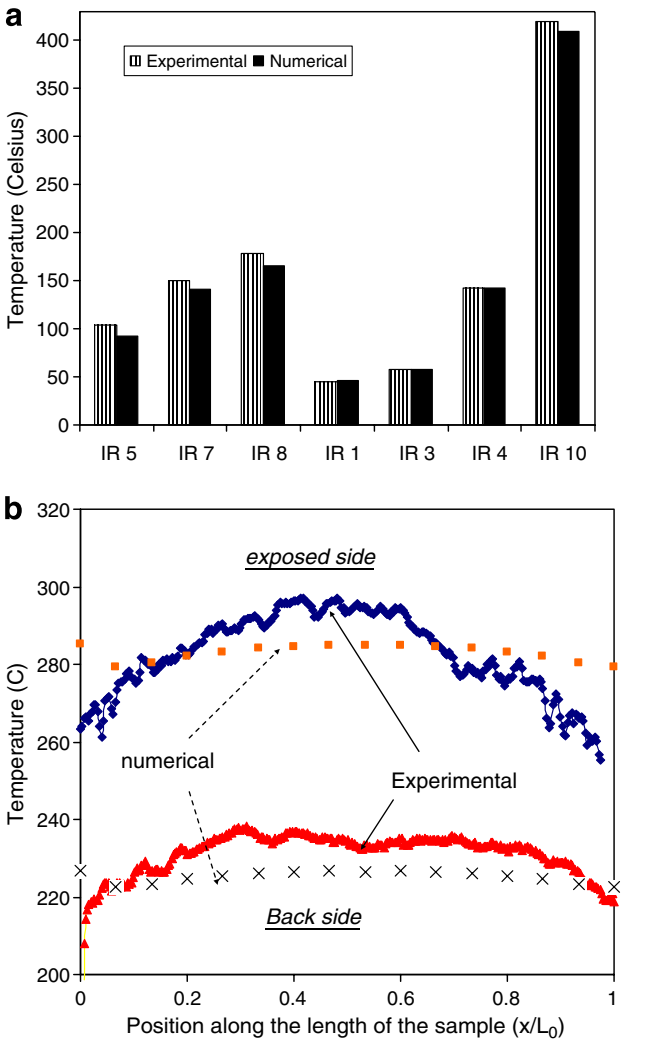


Fig. 12. (a) Experimental and numerical sample surface temperatures of the plate exposed to the radiant heater at temperature $T_s = 280$ °C, 550 °C, and 700 °C. (b) Steady state status for experiment IR 9, experimental and numerical temperature are plotted for the front side and back side.

in Fig. 12b, showing that the model can provide a good correlation on both sides of the plate.

The numerical results are in a good agreement with the experimental results. The largest difference is of 20 °C for a heat source temperature of 550 °C. Generally the prediction is more accurate for a lower heat source. The present model allow one to predict surface temperature of a plate exposed to a heat source in a form of radiant heater with an accuracy of 20 °C in the worst case.

## 9. Discussions and conclusion

The present study developed a model to predict temperature distribution on the surface of a thin composite plate exposed horizontally to a concentrated heat source. This was verified experimentally. The present model is limited to a range of distances of 62–440 mm and heat flux up to 200 W for the gas flame and a temperature of 600 °C for

the radiant heater. Radiant heater supplied heat by radiative mode, where as the flame heated the plate more by heating the surrounding air which then convected the heat to the plate. Flame heating in general heated the plate to higher temperature and the temperature varied non-linearly from the center of the flame to the outside. Such prediction should prove useful to estimate the role of exposing such plate to heat sources on damage caused. The correlation between temperature and damage would then be developed.

## Acknowledgement

We acknowledge the support of Air Force Research Laboratory Contract FA8651-04-C-0303 Composite Fire Safety Initiative for this study.

## References

[1] G.H. Greer, Thermal aging of contemporary graphite/epoxy materials, SAMPE Symp. 24 (1979) 1039.
[2] K.N. Street, A.J. Russell, F. Bonsang, Thermal damage effects on delamination toughness of a graphite/epoxy composite, Compos. Sci. Technol. 32 (1988) 1.
[3] A.P. Mouritz, Z. Mathys, Mechanical properties of fire-damaged glass-reinforced phenolic composites, Fire Mater. 24 (2000) 67–75.
[4] A.P. Mouritz, Z. Mathys, Post fire mechanical properties of marine polymer composites, Compos. Struct. 47 (1999) 643–653.
[5] E. Armstrong-Carroll (Naval Air Warfare Cent), P.A. Mehrkam, R. Cochran, Characterization of heat damage in graphite/epoxy composites, ASTM Special Technical Publication, no. 1274, August 1996, pp. 37–55.
[6] E. Armstrong-Carroll (Naval Air Warfare Cent - Aircraft Div Warminster), P.A. Mehrkam, R. Cochran, Evaluation of the effect of heat damage on bismaleimide composites, in: International SAMPE Technical Conference, vol. 26, 50 Years of Progress in Materials and Science Technology, 1994, pp. 354–364.
[7] H. Nayeb-Hashemi (Northeastern Univ), P. Kisnomo, N. Saniei, Nondestructive evaluation of fiberglass reinforced plastic subjected to localized heat damage, using acoustic emission, in: American Society of Mechanical Engineers, Pressure Vessels and Piping Division (Publication) PVP, vol. 369, Recent Advanced in Solids/Structures and Application of Metallic Materials, 1997, pp. 119–131.
[8] E.G. Henneke II (Va Polytech Inst & State Univ, Blacksburg), K.L. Reifsnider, W.W. Stinchcomb, Thermography and method for damage detection. J. Metals 31(9) (1979) 11–15.
[9] P.A. Mehrkam (Naval Air Warfare Cent), E. Armstrong-Carroll, Detection of composite heat damage by drift spectroscopy, in: International SAMPE Symposium and Exhibition (Proceedings), vol. 38(1), Advanced Materials: Performance Through Technology Insertion, 1993, pp. 217–225.
[10] G.L. Powell (Oak Ridge Y-12 Plant), C.J. Janke, T.E. Barber, Nondestructive inspection of heat damage to graphite–epoxy laminates using diffuse reflectance Fourier transform infrared spectroscopy (DRIFTS), in: International SAMPE Technical Conference, vol. 29, Composites for Real World, 1997, pp. 766–775.
[11] T. Hara, S. Kato, Numerical simulation of thermal plumes in free space using the standard $k$–$\varepsilon$ model, Fire Safety J. 39 (2004) 105–129.
[12] H.-Z. You, An investigation of fire-plume region, Fire Mater. 8 (1) (1984).
[13] R. Ganapathy, Natl Coll, On buoyancy induced heat and mass transfer from a concentrated point source, Fluid Dyn. Res. 11 (5) (1993) 187–196.
[14] V.P. Carey, J.C. Mollendorf, Temperature field above a concentrated heat source on a vertical adiabatic surface, Int. J. Heat Mass Transfer 20 (10) (1977) 1059–1067.
[15] S.G. Tuttle, B.W. Webb, M.Q. McQuay, Convective heat transfer from a partially premixed impinging flame jet. Part I: Time-averaged results, Int. J. Heat Mass Transfer 48 (7) (2005) 1236–1251.
[16] S.G. Tuttle, B.W. Webb, M.Q. McQuay, Convective heat transfer from a partially premixed impinging flame jet. Part II: Time-resolved results, Int. J. Heat Mass Transfer 48 (7) (2005) 1252–1266.
[17] A.D. Johnson, A. Ebbinghaus, T. Imanari, S.P. Lennon, N. Marie, Large-scale free and impinging turbulent jet flames—numerical modelling and experiments, Inst. Chem. Eng. Symp. Ser. (141) (1997) 113–126.
[18] G.K. Malikov, Ye.M. Shleymovich, D.L. Lobanov, Numerical modeling of combined heat transfer in free-jet flames, Heat Transfer Res. 26 (1–2) (1995) 23–28.
[19] L.C. Kwok, C.W. Leung, C.S. Cheung, Heat transfer characteristics of an array of impinging pre-mixed slot flame jets, Int. J. Heat Mass Transfer 48 (9) (2005) 1727–1738.
[20] G.T. Atkinson, D.D. Drysdale, Convective heat transfer from fire gases, Fire Safety J. 19 (2–3) (1992) 217–245.
[21] G. Heskestad, T. Hamada, Ceiling jets of strong fire plumes, Fire Safety J. 21 (1) (1993) 69–82.
[22] H.H. Liakos (Department of Chemical Engineering, Natl. Technical Univ. of Athens), E.P. Karamida, M.A. Founti, N.C. Markatos, Heat and mass transfer study of impinging turbulent premixed flames, Heat and Mass Transfer/Waerme- und Stoffuebertragung 38(4–5) (2002) 425–432.
[23] Z. Zhao, T.T. Wong, C.W. Leung, Impinging premixed butane/air circular laminar flame jet—influence of impingement plate on heat transfer characteristics, Int. J. Heat Mass Transfer 47 (23) (2004) 5021–5031.
[24] K. Mizuno, R. Mital, R. Viskanta, Experimental study of premixed flame impingement heat transfer, in: American Society of Mechanical Engineers, Heat Transfer Division, (Publication) HTD, vol. 335, no. 4, Proceedings of the ASME Heat Transfer Division, 1996, pp. 245–252.
[25] g.K. Hargrave, m. fairweather, j.K. kilham, Forced convective heat transfer from premixed flames—part 2: impingement heat transfer, Int. J. Heat Fluid Flow 8 (2) (1987) 132–138.
[26] S. Chander, A. Ray, Investigation of effect of burner diameter on heat transfer characteristics of methane/air flame impinging on a flat surface, in: Proceedings of the ASME Summer Heat Transfer Conference, vol. 1, Proceedings of the ASME Summer Heat Transfer Conference, HT 2005, pp. 213–220.
[27] S. Chander (Department of Mechanical Engineering, Indian Institute of Technology Delhi), A. Ray, Flame impingement heat transfer: a review, Energy Convers. Manage. 46(18-19) (2005) 2803–2837.
[28] H.-Z. You, An investigation of fire-plume impingement on a horizontal ceiling, Fire Mater. 9 (1) (1985).
[29] R.L. Alpert, Fire Technol. 8 (1972) 181.
[30] J.W. Williamson, A. Marshall, Characterizing the ignition hazard from a cigarette lighter flame, Fire Safety J. (2004).
[31] S. Yokoi, Study on the prevention of fire-spread caused by hot upward current, Report of the Building Research Institute, No. 34, November 1960.
[32] ThermaCAM researcher, FLIR System, Infrared software.
[33] Wintherm® 8.0, Thermal Analysis Software, Thermoanalytics©, Inc.
[34] P. Frank Incropera, D.P. DeWitt, Introduction to Heat Transfer, 3rd ed., p. 684, graph 13.4.